

# Segmentation-free quasi-Newton method for polyenergetic CT reconstruction

T. Humphries and A. Faridani

## I. INTRODUCTION

X-ray polychromaticity is a well-known source of artifacts in clinical CT imaging. As a polyenergetic X-ray beam passes through an object, rays with lower energy are preferentially attenuated, and thus the spectrum of the beam becomes increasingly skewed towards high-energy rays. This *beam hardening* phenomenon results in inconsistent projection data, and produces artifacts in images reconstructed using filtered backprojection (FBP). These artifacts typically appear in the form of *cupping* (underestimation of attenuation coefficients, particularly towards the centre of the object), as well as dark streaking between regions of high attenuation (e.g. bone).

Methods for reducing or eliminating beam hardening artifacts can be broadly categorized into post-reconstruction approaches, which attempt to eliminate artifacts from an image reconstructed using FBP, or iterative reconstruction approaches, which attempt to reconstruct an artifact-free image from the projection data, by incorporating X-ray polychromaticity directly into the system model. In this paper we compare a well-known post-reconstruction approach [1], [2] with our own iterative approach which is based on one presented in [3]. Two numerical phantom experiments are used to demonstrate that the post-reconstruction approach does not compensate for artifacts caused by more than one different type of high attenuation material. The iterative approach is able to reconstruct artifact-free images in both experiments.

## II. METHODOLOGY

### A. Polyenergetic model

For polyenergetic X-ray beams, the projection measurement recorded by the  $i$ th detector can be modeled as

$$\mathbf{P}_i(\boldsymbol{\mu}) = \int P_0(\varepsilon) \exp(-\mathcal{R}_i[\boldsymbol{\mu}(\mathbf{x}, \varepsilon)]) d\varepsilon. \quad (1)$$

Here,  $\varepsilon$  represents beam energy,  $P_0(\varepsilon)$  is the blank scan intensity as a function of energy,  $\boldsymbol{\mu} : \mathbb{R}^2 \times \mathbb{R} \rightarrow \mathbb{R}$  is the energy-dependent attenuation map of the object being imaged,  $\mathbf{x}$  is position, and  $\mathcal{R}_i$  represents the Radon transform of the object along the line normal to detector  $i$ , with  $1 \leq i \leq N_{proj}$ . For the purposes of reconstruction, we discretize the spectrum into  $N_\varepsilon$  energy levels, indexed by  $h$ , and re-weight  $P_0(\varepsilon_h)$  appropriately to approximate the continuous spectrum. The attenuation map  $\boldsymbol{\mu}$  is discretized into  $N_{pix}$  pixels, indexed by  $j$ . The problem is then to use this data to reconstruct an attenuation map of the object at some reference energy,  $\varepsilon_0$ .

### B. Post-reconstruction correction

The post-reconstruction correction [1], [2] is a two-step procedure. The first step is a soft tissue correction where one

simulates monoenergetic data, based on the assumption that the object consists only of soft tissue. One first determines the equivalent length of soft tissue,  $T_i^s$ , that the beam would pass through to generate each measurement  $\mathbf{P}_i$ , by solving the nonlinear equation

$$\mathbf{P}_i = \sum_{h=0}^{N_\varepsilon} P_0(\varepsilon_h) \exp(-\mu_{\text{soft}}(\varepsilon_h) \cdot T_i^s),$$

for all  $i$ . One then simulates monoenergetic projection data,  $\mathbf{M}_i$ , at the reference energy by

$$\mathbf{M}_i = \mu_{\text{soft}}(\varepsilon_0) T_i^s,$$

and reconstructs an image from this data using FBP. This stage tends to produce an image where cupping artifacts are reduced, but streaks caused by bone still exist. In the second stage of the method, one segments this image into regions containing bone and regions containing soft tissue. From this segmentation, one estimates the length of intersection of each ray with bone,  $T_i^b$ . Finally, a new estimate of  $T_i^s$  is generated from solving

$$\mathbf{P}_i = \sum_{h=0}^{N_\varepsilon} P_0(\varepsilon_h) \exp(-\mu_{\text{soft}}(\varepsilon_h) \cdot T_i^s - \mu_{\text{bone}}(\varepsilon_h) \cdot T_i^b).$$

The updated monoenergetic approximation is then

$$\mathbf{M}_i = \mu_{\text{soft}}(\varepsilon_0) T_i^s + \mu_{\text{bone}}(\varepsilon_0) T_i^b,$$

which is used to reconstruct a second image with FBP.

### C. Iterative method

Our iterative method follows that of [3], where the energy dependent values  $\mu(\varepsilon)$  for different materials are modeled as the sum of a photoelectric component and a Compton scattering component. The energy dependencies of the photoelectric effect  $\Phi(\varepsilon)$  and Compton scattering  $\Theta(\varepsilon)$  are

$$\Phi(\varepsilon) = \frac{1/\varepsilon^3}{1/\varepsilon_0^3}, \quad \Theta(\varepsilon) = \frac{f_{KN}(\varepsilon)}{f_{KN}(\varepsilon_0)}, \quad (2)$$

where  $f_{KN}$  is the Klein-Nishina function. We then have

$$\mu(\varepsilon) = \phi \cdot \Phi(\varepsilon) + \theta \cdot \Theta(\varepsilon), \quad (3)$$

where  $\phi$  and  $\theta$  are coefficients which depend on the specific material.

This parameterization would require estimating twice as many parameters as in a typical reconstruction problem. To reduce the number of variables further, [3] suggest modeling  $\theta$  and  $\phi$  as functions of  $\boldsymbol{\mu}$  at the reference energy  $\varepsilon_0$ , rather than as independent quantities. We then have a forward model

$$\widehat{\mathbf{P}}_i(\boldsymbol{\mu}) = \sum_{h=1}^{N_\varepsilon} P_0(\varepsilon_h) \exp[-\mathbf{R}_i(\boldsymbol{\mu}) \cdot \Phi(\varepsilon_h) + \theta(\boldsymbol{\mu}) \cdot \Theta(\varepsilon_h)], \quad (4)$$

TABLE I  
MATERIALS USED IN PHANTOM EXPERIMENTS ALONG WITH THEIR  
ATTENUATION COEFFICIENTS AT 70 KEV (IN  $\text{CM}^{-1}$ ).

$\mu(70 \text{ keV})$	1. Soft	2. Fat	3. Bone	4. Dense
	0.1935	0.1717	0.4974	0.2780

where  $\boldsymbol{\mu}$  is the column vector representing  $\mu(\varepsilon_0)$  for every pixel, and  $\mathbf{R}_i$  is the  $i$ th row of the  $N_{proj} \times N_{pix}$  matrix  $\mathbf{R}$  representing a discrete approximation to the Radon transform.

While [3] incorporate this model into a maximum-likelihood algorithm, we consider the reconstruction problem as one of minimizing the discrepancy between the measured data  $\mathbf{P}_i$  and the forward projection of the estimate,  $\hat{\mathbf{P}}_i$  (Eq. 4), for all  $i$ . Since the parameters to be estimated are exponentiated, we compare the log of the projection data and minimize the function

$$G(\boldsymbol{\mu}) = \|\mathbf{F}(\boldsymbol{\mu})\|_2^2, \text{ where } \mathbf{F}_i(\boldsymbol{\mu}) = \ln \hat{\mathbf{P}}_i(\boldsymbol{\mu}) - \ln \mathbf{P}_i. \quad (5)$$

From the above equations it follows that the gradient of  $G$  is

$$\frac{\partial G(\boldsymbol{\mu})}{\partial \mu_j} = 2 \sum_{i=1}^{N_{proj}} \mathbf{F}_i(\boldsymbol{\mu}) \frac{\partial \mathbf{F}_i(\boldsymbol{\mu})}{\partial \mu_j}, \quad (6)$$

where

$$\frac{\partial \mathbf{F}_i(\boldsymbol{\mu})}{\partial \mu_j} = \frac{-\mathbf{R}_{i,j}}{\hat{\mathbf{P}}_i(\boldsymbol{\mu})} \sum_{h=1}^{N_\varepsilon} P_0(\varepsilon_h) \left[ \Phi(\varepsilon_h) \frac{d\phi}{d\mu_j} + \Theta(\varepsilon_h) \frac{d\theta}{d\mu_j} \right] \times \exp[-\mathbf{R}_i(\boldsymbol{\mu}) \cdot \Phi(\varepsilon_h) + \theta(\boldsymbol{\mu}) \cdot \Theta(\varepsilon_h)]. \quad (7)$$

Given the objective function and its gradient, we can apply a minimization algorithm to solve the reconstruction problem. We use limited-memory bounded BFGS [4], a quasi-Newton approach which uses a Hessian approximation to determine the minimizer of the objective function, and includes the ability to impose a non-negativity constraint on  $\boldsymbol{\mu}$ .

### III. RESULTS AND CONCLUSIONS

We consider two  $200 \times 200$  pixel numerical phantoms. The first is a circular phantom consisting of soft tissue, four small regions containing bone, and an interior region containing fat. The second phantom consists of soft tissue, three bone regions, and three other regions containing air, fat, and a dense material. The measured projection data consisted of 360 views taken over  $180^\circ$  and was generated by averaging projection data over 124 different energy levels according to a weighted spectrum. For the purposes of reconstruction, we assumed only eleven energy levels, and generated the weighting coefficients  $P_0(\varepsilon_h)$  using the composite trapezoid rule.

Figs 1 and 2 show the results of the two approaches for both phantoms, as well as FBP images reconstructed from ideal monoenergetic data and from polyenergetic data. For Phantom 1, which consists only of soft tissue, fat and bone, both methods are able to successfully remove beam hardening artifacts. For Phantom 2, however, only the iterative approach successfully removes all the artifacts. The presence of the region of dense material (denoted (4) in Fig. 2), whose

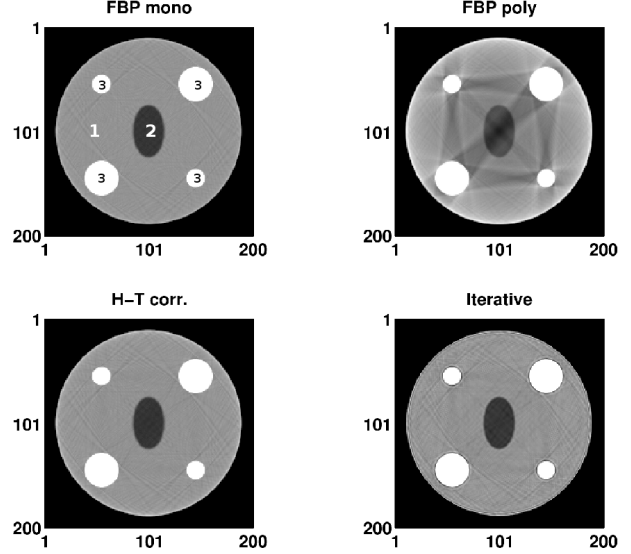


Fig. 1. Reconstructed images of first phantom. Top left: image reconstructed from ideal monoenergetic data, with tissue types labeled (cf. Table I). Top right: image reconstructed from polyenergetic data showing typical beam hardening artifacts. Bottom left: Image reconstructed using post-reconstruction technique. Bottom right: image reconstructed using iterative technique. Iterative image has been smoothed using anisotropic diffusion.

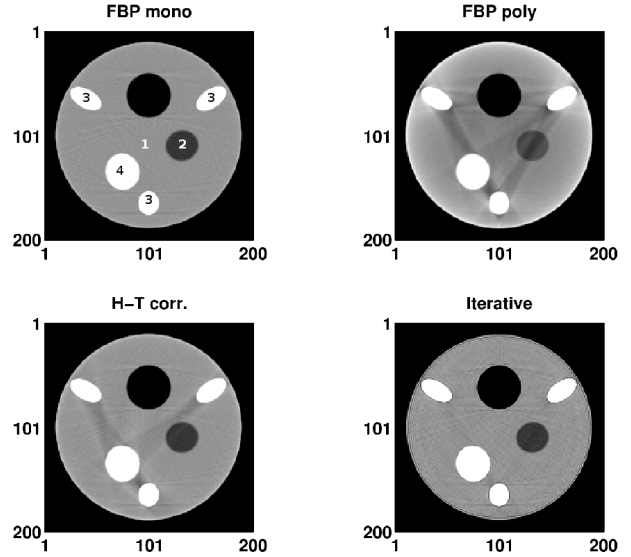


Fig. 2. Reconstructed images of second phantom. See Fig. 1 caption for descriptions.

attenuation coefficient differs significantly from that of bone and soft tissue, produces artifacts that the post-reconstruction correction does not remove. We note that the gradient-based iterative approach presented here does not require any segmentation, is flexible, and can readily incorporate attenuation models other than (3), if appropriate.

### REFERENCES

- [1] P. M. Joseph and R. D. Spital. *Journal of Computer Assisted Tomography*, 2(1):100–108, 1978.
- [2] S. Trivedi and G. Herman. *IEEE Trans. Med. Imag.*, MI-2(3):128–135, 1985.
- [3] B. De Man et al. *IEEE Trans. Med. Imag.*, 20(10):999–1008, 2001.
- [4] R.H. Byrd et al. *SIAM J. Sci. Comput.*, 16(5):1190–1208, 1995.